



Application of the newly developed nutrient diol index (NDI) as a sea surface nutrient proxy in the East Sea for the last 240 years

Jong-Ku Gal^{a,b}, Jung-Hyun Kim^{b,*}, Solbin Kim^a, Sang Han Lee^c, Kyu-Cheul Yoo^b,
Kyung-Hoon Shin^{a,**}

^a Hanyang University, 55 Hanyangdaehak-ro, Sangnok-gu, Ansan, 15588, South Korea

^b Korea Polar Research Institute (KOPRI), 26 Songdomirae-ro, Yeosu-gu, Incheon, 21990, South Korea

^c Korea Research Institute of Standards and Science, 267 Gajeong-ro, Yuseong-gu, Daejeon, 34113, South Korea



ARTICLE INFO

Keywords:

Long chain diols
Nutrient diol index
Surface nutrient proxy
Long chain diol index
Alkenone unsaturation index

ABSTRACT

We assessed the applicability of the nutrient diol index (NDI) as a proxy for sea surface nutrients by analyzing sediments from a box core (ES14-BC03) collected in the southwestern continental slope of the East Sea, or the Japan Sea (hereafter the East Sea). The estimated sedimentation rate based on the ²¹⁰Pb chronology was 0.15 cm yr⁻¹ over the last 240 yrs. The NDI-derived phosphate (0.69 μmol L⁻¹) and nitrate (8.63 μmol L⁻¹) concentrations for the core-top sediment were within the average phosphate (0.26 ± 0.08 μmol L⁻¹) and nitrate (3.38 ± 2.32 μmol L⁻¹) concentration ranges for the last ~20 years, accounting for both estimation error and variation in observational data. The distributions of the NDI-diols varied slightly through time, grouping into two distinct clusters (Cluster 1 and Cluster 2) in both principle component analysis (PCA) and hierarchical clustering of principal components (HCPC). Cluster 2 represented a time period with higher relative abundances of the C₂₈ and C₃₀ 1,14-diols, resulting in higher NDI-derived nutrient concentrations than those of other periods. Interestingly, during this period, the U₃₇^K-derived sea surface temperatures (SSTs) also decreased. These results indicate that higher surface nutrient conditions and colder SSTs occurred between 1884 CE and 1911 CE, which might be associated with stronger upwelling intensity at the study site. This study is the first application of the NDI to a down-core, demonstrating that the NDI can be a useful proxy that provides helpful information about past sea surface nutrient conditions.

1. Introduction

Marine nutrients control primary productivity, making them useful proxies for recording the ventilation of deep-water masses (e.g., Marchitto, 2013 and references therein). Currently, several proxies are commonly used to reconstruct paleonutrients: foraminiferal δ¹³C, Cd/Ca, Ba/Ca, and Zn/Ca; and organic matter δ¹⁵N. Epibenthic foraminiferal δ¹³C has been used as a tracer of phosphate nutrient concentrations (Kroopnick, 1985; Duplessy et al., 1984; Lynch-Stieglitz and Marchitto, 2014). Trace elements such as Cd, Zn, and Ba are incorporated into foraminiferal calcite during precipitation (e.g., Boyle, 1981; Hendry et al., 2008; Bryan and Marchitto, 2010). Hence, epibenthic foraminiferal Cd/Ca, Zn/Ca and Ba/Ca have been used as tracers of phosphate and silicate nutrient concentrations, and total alkalinity, respectively (e.g., Boyle and Keigwin, 1987; Lea and Boyle, 1990; Marchitto et al., 2002; Marchitto and Broecker, 2006). δ¹⁵N values of

organic matter reflect nutrient utilization in surface waters (e.g., Galbraith et al., 2008). Accordingly, these inorganic and organic proxies can be used to reconstruct deep-water nutrient conditions or surface nutrient utilization, but not surface nutrient supply.

Long chain alkyl diols (LCDs) are composed of a long alkyl chain (≥ 28 C atoms) with alcohol groups at C₁ and a mid-chain position (e.g., carbon numbers 13, 14, 15). In marine sediments, the major LCDs are C₂₈ and C₃₀ 1,13-diols, as well as C₃₀ and C₃₂ 1,15-diols (e.g., De Leeuw et al., 1981; Versteegh et al., 1997; Rampen et al., 2012). C₂₈ and C₃₀ 1,14-diols are also ubiquitous in marine sediments (e.g., Rampen et al., 2008, 2014; Willmott et al., 2010). Recently, Gal et al. (2018) proposed the nutrient diol index (NDI) as a quantitative surface nutrient proxy based on LCD ratios using C₂₈ 1,14-diol and C_{28:1} 1,14-diol in the numerator and 1,13-, 1,14-, and 1,15-diols (excluding the C₃₂ 1,15-diol) in the denominator. They found that NDI values were positively correlated with surface water phosphate and nitrate concentrations for suspended

* Corresponding author.

** Corresponding author.

E-mail addresses: jhkim123@kopri.re.kr (J.-H. Kim), shinkh@hanyang.ac.kr (K.-H. Shin).

<https://doi.org/10.1016/j.quaint.2018.11.003>

Received 18 May 2018; Received in revised form 7 October 2018; Accepted 5 November 2018

Available online 12 November 2018

1040-6182/ © 2018 Elsevier Ltd and INQUA. All rights reserved.

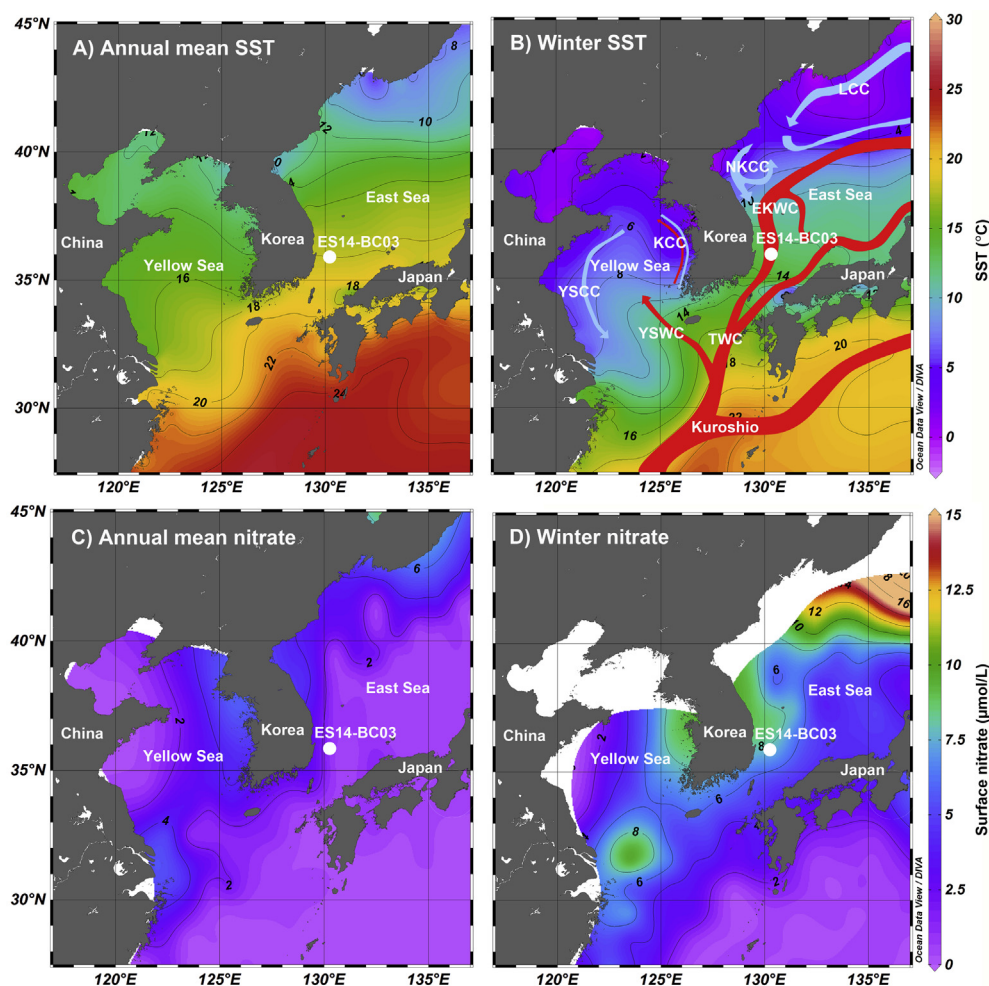


Fig. 1. (A) Annual mean SSTs in the study area. (B) Schematic diagram of main surface currents (Senjyu, 1999) in the East Sea on top of winter SST values. (C) Annual mean nitrate concentration. (D) Winter nitrate concentrations obtained from the World Ocean Atlas (WOA13) (Locarnini et al., 2013; Garcia et al., 2013). Current names are labeled in panel B. TWC: the Tsushima Warm Current, EKWC: the East Korean Warm Current, NKCC: the North Korean Cold Current, LCC: Liman cold current, KCC: Korean coastal current, YSCC: Yellow Sea Coastal Current, YSWC: Yellow Sea Warm Current. (For interpretation of the references to color in this figure legend, the reader is referred to the Web version of this article.)

particulate matter (SPM) along a South-North transect from the East Sea to the Bering Sea as well as for global surface sediment data. However, the potential for the NDI to serve as a paleo-nutrient proxy for estimating changes in sea surface nitrate (or phosphate) concentrations from sediment cores has not yet been evaluated.

In this study, we assessed for the first time the applicability of the NDI for reconstructing sea surface nutrient conditions by analyzing a sediment core collected in the southwestern continental slope of the East Sea. In addition, to obtain additional information on the past oceanic conditions, we reconstructed sea surface temperatures (SSTs) using the alkenone unsaturation index (U_{37}^K) and the long chain diol index (LDI).

2. Materials and methods

2.1. Site description and sample collection

The East Sea is a semi-enclosed marginal sea influenced by the Tsushima Warm Current (TWC), which is characterized by warm temperature above 14.0 °C and salinity higher than 34.4 (e.g., Park et al., 2004; Kim et al., 2005, Fig. 1). In the Korea Strait, part of the Tsushima Warm Current (TWC) forms the East Korean Warm Current (EKWC), which moves northward along the east coast of Korea. The North Korean Cold Current (NKCC) flows southward along the North Korean coast and joins the EKWC around 38°N. The two currents, now joined, then flow eastward, comprising the Polar Front. In general, the mean surface temperature is low in winter and high in summer ranging from 8.0 to 26.3 °C, while surface salinity is high in winter and low in

summer varying between 33.3 and 34.4 (Joo et al., 2014). The major inorganic nutrient concentrations such as nitrate, phosphate and silicate in winter are approximately 2–3 times higher than in summer (Joo et al., 2014). The primary productivity in the Ulleung Basin of the East Sea is markedly higher than adjacent regions such as the Japan Basin (e.g., Yamada et al., 2005; Yoo and Park, 2009), with the highest primary productivity in spring (April to May) (Joo et al., 2014). In general, southeasterly winds between the low pressure on the Asian continent and the Northwest Pacific high pressure prevail over the study area in summer. Upwelling at the southeastern coast around 35.5°N under upwelling-favorable wind conditions can be maintained a few hours to two weeks, and the resulting cold water masses can be observed by satellite-observed SST measurements (Park and Kim, 2010).

A box core (ES14-BC03) was taken from the southern continental slope in the southwestern part of the East Sea (35°54.68'N, 130°12.68'E, 1383 m water depth) during a test cruise with R/V ARAON, the South Korean icebreaker, in August 2014 (Fig. 1). A 42 cm sub-core was collected with an acrylic tube. The core sediments were fine-grained and had dark greenish grey (0–4 cm), dark grey (4–10 cm), and greyish olive green colors (10–42 cm). The sub-core was sliced at 1-cm intervals on board and placed in pre-combusted glass bottles. Samples were stored at –20 °C, transferred to the laboratory with dry ice, and stored at –20 °C for geochemical analyses.

2.2. Radioisotope analyses

For the box core, ^{210}Pb ($t_{1/2} = 22.3$ yr) activities were indirectly measured using the ^{210}Po method (Nittroer et al., 1979; Santschi et al.,

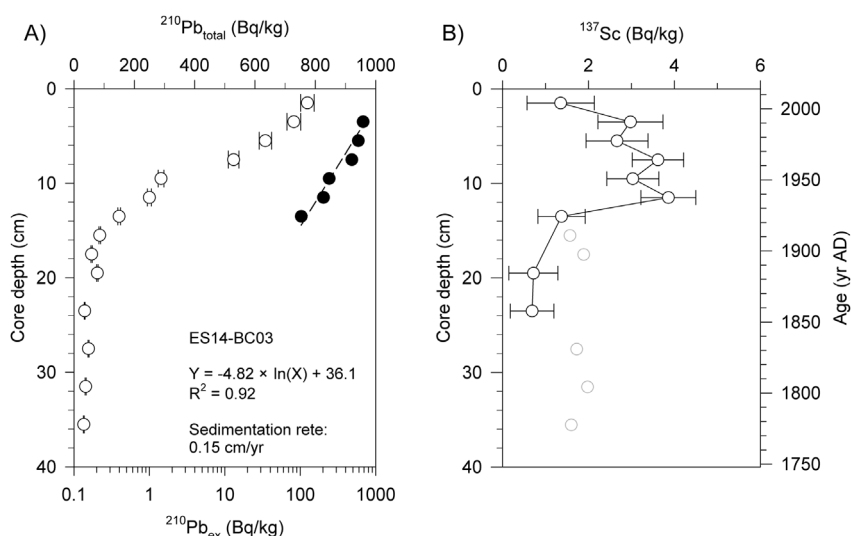


Fig. 2. Downcore profiles of (A) $^{210}\text{Pb}_{\text{total}}$ (open circles) and $^{210}\text{Pb}_{\text{ex}}$ (filled circles) and (B) ^{137}Cs . The horizontal filled grey bar indicates the surface mixed layer. Error bars denote standard deviations. Data without error bars (grey circles) were obtained from only one measurement and thus were not considered in this study due to analytical uncertainties.

2001), in which ^{210}Po and ^{210}Pb are assumed to be in secular equilibrium. About 500 mg of powdered sediments were spiked with ^{209}Po and digested with concentrated HNO_3 on the hot plate by heating at 140°C . Po isotopes (^{209}Po and ^{210}Po) were treated in an acid solution (0.5M HCl) with ascorbic acid and spontaneously deposited onto silver disks at 70°C for 6 h while stirring. The activities of the Po isotopes were counted over the course of two days to get over 1000 measurements with an alpha spectrometer equipped with low background silicon surface barrier detectors (PIPS detector, Canberra, USA) at the Korea Basic Science Institute (KBSI). Measurements were taken at 2-cm interval between 0 and 20 cm core depth and at 4-cm interval between 20 and 42 cm core depth. Determination of excess activity of ^{210}Pb ($^{210}\text{Pb}_{\text{ex}}$) was calculated by subtraction of supported level values ($^{210}\text{Pb}_{\text{sup}}$) from total activity ($^{210}\text{Pb}_{\text{total}}$). Supported values were determined assuming that the activity at the depth of the core where $^{210}\text{Pb}_{\text{total}}$ becomes asymptotic. The apparent sedimentation rate was determined primarily from the excess ^{210}Pb distribution below the zone of the surface sediment mixed layer using the constant rate of supply (CRS) model (Appleby and Oldfield, 1978) based on a slope of the logarithmic regression line (Fig. 2A) as follows:

$$\text{Apparent sedimentation rate} = -\lambda/b \text{ (cm yr}^{-1}\text{)} \quad (1)$$

Where λ is the radioisotope decay constant (^{210}Pb , 0.0311 yr^{-1}) and b is the slope of the regression line.

To verify the average sedimentation rate estimated using ^{210}Pb , ^{137}Cs ($t_{1/2} = 30.05 \text{ yr}$ based on LNHB, 2017) was also analyzed in the same samples (Fig. 2B). The analysis of ^{137}Cs was performed using a gamma spectrometer (AMETEK ORTEC, USA) at the Korea Research Institute of Standards and Science (KRISS) as described by Lee et al. (2018).

2.3. Lipid analysis

Sediment samples were freeze-dried and homogenized using an agate mortar. Sediments ($\sim 1 \text{ g}$) were extracted using an accelerated solvent extractor (Dionex ASE 200, Dionex Corporation, Sunnyvale, CA) with a solvent mixture of 9:1 (v:v) dichloromethane (DCM) to methanol (MeOH) at a temperature of 100°C and a pressure of 1000 psi. The purification of the total lipid extract and the gas chromatography analysis were performed as described by Gal et al. (2018). In brief, the total lipid extracts were separated into three fractions over an Al_2O_3 (activated for 2 h at 150°C) column. The fractions were eluted using hexane:dichloromethane (DCM, 9:1 v:v), hexane:DCM (1:1 v:v), and DCM:methanol (MeOH, 1:1 v:v) as eluents, respectively. The fraction of DCM:MeOH (1:1 v:v) was silylated with N,O-bis(trimethylsilyl)

trifluoroacetamide (BSTFA) and pyridine, and analyzed for LCDs using an Agilent 5977E GC/MSD (Agilent Technologies, Santa Clara, CA) fitted with an HP-5 column ($30 \text{ m} \times 0.25 \text{ mm}$, $0.25 \mu\text{m}$, Agilent). In addition, the fraction of hexane:DCM (1:1 v:v) was analyzed for alkenones using a Shimadzu GC (Shimadzu Corporation, Kyoto, Japan) with a DB-5 column ($60 \text{ m} \times 0.25 \text{ mm}$, $0.25 \mu\text{m}$, Agilent).

The NDI and NDI-derived nutrient concentrations were calculated as described by Gal et al. (2018) as follows:

$$\text{NDI} = \frac{[\text{C}_{28} \text{ 1,14}] + [\text{C}_{28:1} \text{ 1,14}]}{[\text{C}_{28} \text{ 1,14}] + [\text{C}_{28:1} \text{ 1,14}] + [\text{C}_{30} \text{ 1,14}] + [\text{C}_{30:1} \text{ 1,14}] + [\text{C}_{28} \text{ 1,13}] + [\text{C}_{30} \text{ 1,13}] + [\text{C}_{30} \text{ 1,15}]} \quad (2)$$

$$\text{NDI} = 0.413 \times [\text{phosphate}] + 0.015 \quad (R^2 = 0.85, n = 216, p < 0.0001) \quad (3)$$

$$\text{NDI} = 0.026 \times [\text{nitrate}] + 0.075 \quad (R^2 = 0.80, n = 216, p < 0.0001) \quad (4)$$

The long chain diol index (LDI) was calculated using the fractional abundances of LCDs as described by Rampen et al. (2012) and LDI values were converted into SSTs using the equation of Rampen et al. (2012) as follows:

$$\text{LDI} = \frac{[\text{C}_{30} \text{ 1,15}]}{[\text{C}_{28} \text{ 1,13}] + [\text{C}_{30} \text{ 1,13}] + [\text{C}_{30} \text{ 1,15}]} \quad (5)$$

$$\text{LDI} = 0.033 \times \text{SST} + 0.095 \quad (R^2 = 0.969; n = 162) \quad (6)$$

The U_{37}^K values were obtained using the fractional abundances of alkenones as described by Prahl and Wakeham (1987) and SSTs were calculated using the equation presented by Müller et al. (1998) as follows:

$$U_{37}^K = \frac{[\text{C}_{37:2}]}{[\text{C}_{37:2} + \text{C}_{37:3}]} \quad (7)$$

$$U_{37}^K = 0.033 \times T + 0.044 \quad (8)$$

2.4. Statistical analyses

The fractional abundances of each diol component were obtained by normalizing each diol concentration to the summed concentration of all of the alkyl diols considered. Principle component analysis (PCA) and

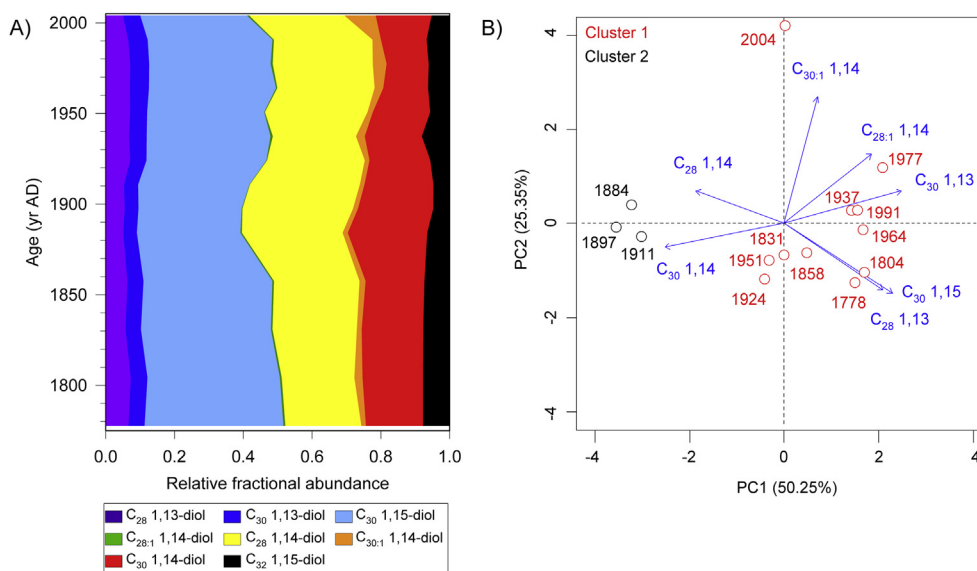


Fig. 3. (A) Relative fractional abundances of individual alkyl diols relative to all eight of the alkyl diols. (B) Principal component analysis (PCA) biplots with the results of the Hierarchical Clustering on Principal Components (HCPC) of the fractional abundances of the alkyl diols except for C₃₂ 1,15-diol.

hierarchical clustering of principal components (HCPC) were performed on the relative fractional abundances of LCDs in R (R Core team, 2015). In addition, the *t*-test was performed using the SPSS 12.0 software (SPSS Inc. Chicago, IL) and the result was represented as mean ± standard deviation (SD).

3. Results

Measured ²¹⁰Pb_{total} activities ranged from 33 to 774 Bq kg⁻¹ of dry sediment weight and measured ²¹⁰Pb_{sup} activities for sediment between 16 and 36 cm had an average value of 54 ± 21 Bq kg⁻¹ (Fig. 2A). The surface sediment mixed layer was identified in terms of sharp changes in sediment color and ²¹⁰Pb_{ex} gradient at 4 cm core depth. The average sedimentation rate was 0.15 cm yr⁻¹. The activity concentrations of ¹³⁷Cs ranged from 0.7 to 3.9 Bq kg⁻¹. The highest concentrations of ¹³⁷Cs were found at a core depth of 11–12 cm (Fig. 2B).

The saturated and unsaturated C₂₈, C₃₀, and C₃₂ alkyl diols with mid-chain positions at 13, 14, and 15 were identified and quantified. The C₃₀ 1,15-diol was the most dominant LCD followed by C₂₈ 1,14-diol and C₃₀ 1,14-diol (Fig. 3A, Table 1). In contrast, the relative abundances of C_{30:1} 1,14-diol and C_{28:1} 1,14-diol were small throughout the whole core (Fig. 3A, Table 1). NDI values varied between 0.235 and

0.340, and the resulting phosphate and nitrate concentrations were 0.53–0.79 and 6.16–10.19 μmol L⁻¹, respectively (Fig. 4A–B). LDI values ranged from 0.737 to 0.787, corresponding to 19.4–21.0 °C (Fig. 4C). U₃₇^K values varied between 0.674 and 0.743 and their corresponding calculated SSTs ranged from 19.1 to 21.2 °C (Fig. 4D).

4. Discussion

4.1. ²¹⁰Pb geochronology

Excess activities (²¹⁰Pb_{ex}) at a core depth of 4–14 cm were between 150 and 729 Bq kg⁻¹ and decreased logarithmically with depth (Fig. 2A). The regression line was thus fit from 4 to 14 cm of the core. The slope of the ²¹⁰Pb_{ex} profile had a determinant coefficient (R²) of 0.92. The estimated sedimentation rate for the last 240 years (1770 CE to 2010 CE) was 0.15 cm yr⁻¹. Previous studies based on ²¹⁰Pb_{ex} profiles in the southwestern part of the East Sea estimated apparent sedimentation rates at 0.02 and 0.2 cm yr⁻¹, and reported a decreasing trend with increasing water depth (e.g., Hong et al., 1997; Cha et al., 2005, 2007; Lee et al., 2008). Thus, our estimate is well within the range of previous findings on the southern continental slope in the southwestern part of the East Sea.

Table 1
Relative fractional abundances of individual long chain diols (LCDs) and calculated diol indices.

Core depth (cm)	Age (yr AD)	Relative fractional abundances								NDI	NDI-derived phosphate (μmol/L)	NDI-derived nitrate (μmol/L)	LDI	LDI-derived temperature (°C)	Cluster
		C _{28:1} 1,14	C ₂₈ 1,14	C ₂₈ 1,13	C ₃₀ 1,15	C _{30:1} 1,14	C ₃₀ 1,14	C ₃₀ 1,13	C ₃₂ 1,15						
0–1	2004	0.01	0.28	0.05	0.31	0.09	0.16	0.05	0.05	0.299	0.69	8.63	0.756	20.0	1
2–3	1991	0.00	0.29	0.07	0.36	0.02	0.13	0.06	0.07	0.312	0.72	9.11	0.749	19.8	1
4–5	1977	0.01	0.29	0.07	0.35	0.04	0.12	0.05	0.06	0.317	0.73	9.29	0.737	19.4	1
6–7	1964	0.00	0.28	0.07	0.37	0.03	0.13	0.06	0.06	0.306	0.70	8.87	0.746	19.7	1
10–11	1951	0.00	0.30	0.07	0.34	0.02	0.17	0.05	0.06	0.318	0.73	9.36	0.739	19.5	1
12–13	1937	0.01	0.24	0.07	0.36	0.03	0.17	0.05	0.08	0.271	0.62	7.53	0.752	19.9	1
14–15	1924	0.00	0.28	0.07	0.35	0.01	0.18	0.05	0.06	0.303	0.70	8.78	0.746	19.7	1
16–17	1911	0.00	0.32	0.05	0.32	0.01	0.20	0.04	0.05	0.337	0.78	10.09	0.774	20.6	2
18–19	1897	0.00	0.32	0.06	0.30	0.01	0.22	0.04	0.05	0.340	0.79	10.19	0.759	20.1	2
20–21	1884	0.00	0.29	0.05	0.30	0.01	0.23	0.04	0.07	0.318	0.73	9.34	0.769	20.4	2
24–25	1858	0.00	0.25	0.06	0.37	0.02	0.17	0.05	0.07	0.274	0.63	7.64	0.773	20.6	1
28–29	1831	0.00	0.25	0.06	0.38	0.01	0.18	0.04	0.08	0.271	0.62	7.53	0.787	21.0	1
32–33	1804	0.01	0.21	0.07	0.38	0.02	0.18	0.05	0.08	0.235	0.53	6.16	0.761	20.2	1
36–37	1778	0.01	0.22	0.07	0.40	0.01	0.17	0.05	0.08	0.245	0.56	6.55	0.782	20.8	1

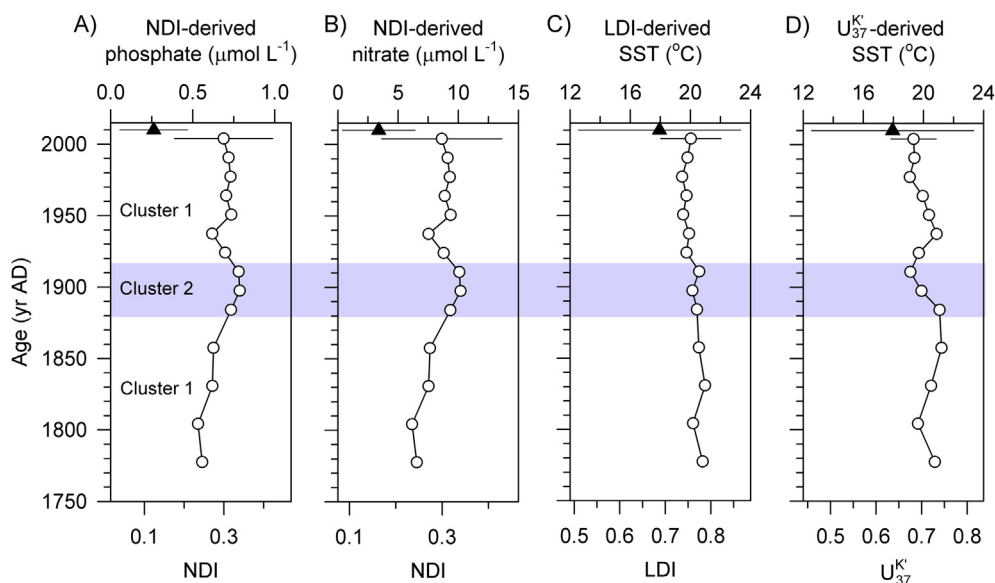


Fig. 4. Downcore profiles of (A) NDI and NDI-derived phosphate, (B) NDI and NDI-derived nitrate, (C) LDI and LDI-derived SSTs, and (D) U_{37}^{K1} and U_{37}^{K2} -derived SSTs. Filled triangles show the average values for about 20 years obtained from Korea Ocean Data Center (KODC, <http://kodc.nifs.go.kr>). Note that the bars for the average values (filled triangle) and the core-top sediment (open circle) indicate the 1σ standard deviation of the observational dataset (KODC, <http://kodc.nifs.go.kr>) and the estimation error ranges (Gal et al., 2018), respectively.

The ^{137}Cs activity at our continental slope site is lower ($< 4 \text{ Bq kg}^{-1}$, Fig. 2B) than those previously reported on the northern continental slope and in the Ulleung Basin ($> 5 \text{ Bq kg}^{-1}$, Lee et al., 1998; Hong et al., 1999). The peak activity of ^{137}Cs was found at a core depth of 11–12 cm, corresponding to 1937 CE as derived from the ^{210}Pb chronology (Fig. 2B). A previous study on the northern continental slope and in the Ulleung Basin in the East Sea reported a maximum ^{137}Cs concentration at 2–4 cm core depth, corresponding to 1950–1975 CE based on ^{210}Pb (Lee et al., 1998). Large amounts of ^{137}Cs were released into the ocean following frequent nuclear tests during the early 1960s (Palinkas and Nittrouer, 2007) and the Chernobyl NPP accident (ca. 85 PBq) in the former Soviet Union (Devell et al., 1995; De Cort et al., 1998; UNSCEAR, 2000). Fallout of ^{137}Cs began in about 1954 (Peirson, 1971). ^{137}Cs activity profiles in the East China Sea have shown two prominent peaks in 1963 and 1986 associated with the maximum fallout from the atmospheric nuclear tests during the 1960s and the Chernobyl accident, respectively (Zhang et al., 2018). Similarly, if we assume that the highest ^{137}Cs peak found in our core corresponds to the maximum fallout at 1963, there is a difference of ~ 26 years in comparison to that from the ^{210}Pb chronology. Therefore, we consider 26 years to be the age uncertainty of the core in this study.

4.2. Distribution of sedimentary LCDs

All the NDI-diols were quantifiable in the samples investigated (Fig. 3A). The identification of all the NDI-diols in our study is consistent with previous results obtained from suspended particulate matter (SPM) samples collected in the East Sea in July 2015 (Gal et al., 2018). Station T-1 (35.56°N, 130.42°E) in the study by Gal et al. (2018) is near our core site ES14-BC03. However, the T-1 SPM sample showed a different LCD composition than that in our core-top sediment. For the T-1 SPM sample, the C_{30} 1,15-diol (fractional abundance: 0.26) was the most dominant followed by C_{28} 1,14-diol (0.25) and C_{32} 1,15-diol (0.21). In contrast, for our core-top sediment, C_{30} 1,15-diol (0.31), C_{28} 1,14-diol (0.28) and C_{30} 1,14-diol (0.16) were the most dominant LCDs. In particular, the fractional abundance of the C_{30} 1,14-diol was only 0.02 for the T-1 SPM sample while that of the C_{32} 1,15-diol was minor (0.05) for the core-top sediment.

Oxic degradation that occurs as particles sink through the water

column and deposit on the seafloor could be one possible cause of the disparity between reported core-top and SPM LCD compositions. A recent study conducted in the Arabian Sea reported that surface sediments collected in close lateral proximity had decreasing LCDs with increasing oxygen exposure time, suggesting increased oxic degradation (Rodrigo-Gámiz et al., 2016). The oxygen concentration in the East Sea is very high throughout the water column due to rapid ventilation, which is much higher than anywhere else in the Pacific Ocean (Talley et al., 2006). This makes it more likely that LCDs might be influenced by the oxic conditions at our core site. To explore this possibility, we calculated the NDI using the published data by Rodrigo-Gámiz et al. (2016). The resulting NDI values of the sediments under the oxic condition (0.320 ± 0.021) were significantly higher than those of the sediments under the oxygen minimum zone (0.272 ± 0.010) (t -test, $p = 0.021$). Similarly, we may expect higher NDI values of the core-top sediment than that of the SPM sample, if LCDs were affected by the oxic degradation at our core site. However, the NDI value (0.345) obtained from the T-1 SPM (Gal et al., 2018) was very close to that of the core-top sediment (0.299), despite the differences in general composition. This suggests that oxic degradation may be lower at our core site but this possibility has to be further assessed in future.

Another possible cause for the difference in core-top values and SPM values could be related to the seasonality of NDI-diol production. The two different sample types represent different time scales: the SPM sample shows a snapshot signal (seasonal) while the core-top sediment signal is integrated over a longer time period (multi-annual to decadal). The average phosphate and nitrate concentrations for the site (36.08°N, 130.62°E) between 1994 and 2016 (Korea Ocean Data Center (KODC), <http://kodc.nifs.go.kr>) were 0.26 ± 0.08 and $3.38 \pm 2.32 \mu\text{mol L}^{-1}$, respectively (Fig. 4). These average nutrient concentrations from the observational dataset were slightly lower than the NDI-derived values for the T-1 SPM sample (0.80 and $10.37 \mu\text{mol L}^{-1}$, respectively, Gal et al., 2018). They were also lower than the NDI-derived values from the core-top sediment of ES14-BC03 (0.69 and $8.63 \mu\text{mol L}^{-1}$, respectively, Fig. 4A–B). However, the core-top data fall within the ranges of the observational data when considering variation in observational data (KODC, <http://kodc.nifs.go.kr>) and the estimation error ranges provided by Gal et al. (2018). Accordingly, these observations suggest that the NDIs reflect a long-term integrated signal which should be

considered when interpreting reconstructed nutrient records.

4.3. Variations in surface nutrient concentrations for the last 240 years

The distributions of the NDI-diols varied slightly through time (Fig. 3A). To characterize this variation, we performed PCA (Fig. 3B). The first two components of the PCA based on the NDI-diols accounted for 75.6% of variance in the data. On the first principal component (PC1, explaining 50.25% of the variance), the loading of the C_{28} and C_{30} 1,14-diols was opposite to that of all the other NDI-diols. A hierarchical clustering of principal components (HCPC) analysis run on the PCA results revealed two distinct clusters: Cluster 1 and Cluster 2. Cluster 2 included the samples with high relative abundances of C_{28} and C_{30} 1,14-diols. Interestingly, Cluster 2 represented the time period between 1884 CE and 1911 CE, when the NDI values (0.332 ± 0.012) were slightly higher than those of other periods (0.286 ± 0.029 ; Fig. 4). Accordingly, Cluster 2 encompassed a period with higher NDI-derived phosphate ($0.767 \pm 0.029 \mu\text{mol L}^{-1}$) and nitrate concentrations ($9.873 \pm 0.461 \mu\text{mol L}^{-1}$) than those of other periods (0.657 ± 0.070 and $8.133 \pm 1.114 \mu\text{mol L}^{-1}$, respectively).

In marginal seas, such as the East China Sea, a nutrient supply might be enhanced through increased riverine inputs. The Changjiang River (Yangtze River), which flows into the East China Sea, is one of the largest rivers in the world. Freshwater, accompanying nutrients, and suspended particulate matters from Changjiang River can reach the western Jeju Island (Wu et al., 2003, 2007; Gao et al., 2015; Kim et al., 2016), at which point they can be further entrained into the southwestern part of the East Sea via the Tsushima Warm Current (see Fig. 1). Korean rivers (e.g., the Nakdong River) can also supply sediments and riverine nutrients into the East Sea (Cha et al., 2007). C_{32} 1,15-diol has been proposed to be a potential indicator for tracing riverine inputs (De Bar et al., 2016; Lattaud et al., 2017). Therefore, we might expect a positive relationship between the NDI values and C_{32} 1,15-diol abundances with large riverine inputs. In our dataset, however, NDI had a negative relationship with C_{32} 1,15-diol ($R^2 = 0.74$), potentially indicating that riverine nutrients played a minor role in NDI variations in the study area.

An alternative source of a high nutrient supply to the study site is deep water, called the East Sea Proper Water, formed by wintertime deep convection and brine rejection south of Vladivostok (Talley et al., 2006). Some of this deep water spreads southward to the Ulleung Basin (Kim and Seung, 1999; Senjyu et al., 2005), which is connected to the subpolar front. The subpolar front in the western part of the East Sea is found between 41°N and 36°N depending on the year (Choi et al., 2009). Wind-driven upwelling in the southeast coast of Korea has frequently been observed to supply nutrients that enhance primary production (Kwak et al., 2013; Joo et al., 2014). Increased fluxes of 1,14-diols during periods of upwelling in the Arabian Sea correlated with an increase in *Proboscia* diatoms (e.g., Rampen et al., 2007). Therefore, it is possible that increases in C_{30} 1,14-diol and C_{28} 1,14-diol indicate an increase in nutrient supply (Gal et al., 2018) that could come from the production of *Proboscia* diatoms which may be affected by upwelling at the study site during the Cluster 2 period (c.f. Rampen et al., 2014). The Cluster 2 period with higher NDI values coincided with a decrease in U_{37}^K -derived SSTs (Fig. 4). Considering, upwelling events in the southwestern part of the East Sea occur in summer (May–July) and the alkenone concentration and flux in the East Sea increase in spring (April) and summer (June–October) (Lee et al., 2011, 2014), variation in SST may also be associated with increased upwelling intensity. Notably, the LDI-derived SSTs did not show the same cooling during the Cluster 2 period. This could be due to the seasonal differences in production of alkenones and LCDs. These environmental and biological factors should be further evaluated in future research.

Changes in surface nutrient concentrations and SSTs derived from the NDI and paleothermometers (U_{37}^K and LDI) may be associated with

upwelling intensity controlled by the coastal wind strength changes in the East Sea (Park and Kim, 2010). The atmospheric changes observed in the southwestern part of the East Sea over the past 240 years are likely related to a shift in regional climate modes, such as Pacific Decadal Oscillation. However, it is currently difficult to decipher underlying mechanisms directly connecting our records with such climate modes on decadal time scales due to insufficient time resolution and age uncertainties of the records generated from our core sample. Nonetheless, the multi-proxy approach for reconstructing variations in surface nutrient conditions using the newly developed surface nutrient proxy (i.e. NDI) in addition to SST estimates appears to be useful for elucidating mechanisms responsible for past climate change.

5. Conclusions

We applied a newly proposed surface nutrient proxy, the NDI, to a sediment core collected in the southwestern continental slope of the East Sea. The estimated sedimentation rate based on ^{210}Pb chronology was 0.15 cm yr^{-1} over the last 240 yrs (1770–2010 CE). All the LCDs necessary for calculating the NDI were detected in the sediments analyzed. The NDI-derived phosphate and nitrate concentrations for the core-top sediment fall to the ranges of the observational data for the last ~20 years when considering estimation error and observational data variation. The PCA and the subsequent HCPC grouped samples into two distinct clusters (Cluster 1 and Cluster 2). Cluster 2 had higher relative abundances of the C_{28} and C_{30} 1,14-diols during the time period from 1884 CE to 1911 CE, when the NDI values and thus the NDI-derived nutrient concentrations were slightly higher than in other periods. Interestingly, during the Cluster 2 period, the U_{37}^K -derived SSTs were lower, suggesting that higher nutrients and cooler SSTs might be related to stronger upwelling at the study site. Consequently, our study demonstrates that the NDI can be a useful proxy for reconstructing surface nutrient conditions in the past. Nonetheless, more studies should be carried out in order to further validate the NDI as a paleo surface nutrient proxy.

Acknowledgments

This study was supported by the project ‘Deep Water Circulation and Material Cycling in the East Sea (0425-20170025)’ funded by the Ministry of Oceans and Fisheries and a National Research Foundation of Korea (NRF) grant funded by the Ministry of Science and ICT (MSIT) (NRF-2016R1A2B3015388, PN18100).

References

- Appleby, P.G., Oldfield, F., 1978. The calculation of lead-210 dates assuming a constant rate of supply of unsupported ^{210}Pb to the sediment. *Catena* 5, 1–8.
- Boyle, E.A., 1981. Cadmium, zinc, copper, and barium in foraminifera tests. *Earth Planet. Sci. Lett.* 53, 11–35.
- Boyle, E.A., Keigwin, L., 1987. North Atlantic thermohaline circulation during the past 20,000 years linked to high-latitude surface temperature. *Nature* 330, 35–40.
- Bryan, S.P., Marchitto, T.M., 2010. Testing the utility of paleonutrient proxies Cd/Ca and Zn/Ca in benthic foraminifera from thermocline waters. *G-cubed* 11, Q01005.
- Cha, H.J., Lee, C.B., Kim, B.S., Choi, M.S., Ruttnerberg, K.C., 2005. Early diagenetic redistribution and burial of phosphorus in the sediments of the southwestern East Sea (Japan Sea). *Mar. Geol.* 216, 127–143.
- Cha, H.J., Choi, M.S., Lee, C.B., Shin, D.H., 2007. Geochemistry of surface sediments in the southwestern East/Japan Sea. *J. Asian Earth Sci.* 29, 685–697.
- Choi, B.J., Haidvogel, D.B., Cho, Y.K., 2009. Interannual variation of the Polar Front in the Japan/East Sea from summertime hydrography and sea level data. *J. Mar. Syst.* 78, 351–362.
- De Bar, M.W., Dorhout, D.J.C., Hopmans, E.C., Rampen, S.W., Sinnighe Damsté, J.S., Schouten, S., 2016. Constraints on the application of long chain diol proxies in the Iberian Atlantic margin. *Org. Geochem.* 101, 184–195.
- De Cort, M., Dubois, G., Fridman, Sh D., Germenchuk, M.G., Izrael, Yu A., Janssens, A. De, Jones, A.R., Kelly, G.N., Kvasnikova, E.V., Matveenko, I.I., Nazarov, I.M., Yu, P., Sitak, V.A., Stukin, E.D., Tabachny, L. Ya, Tsaurov, Yu S., Avdyushin, S.I., 1998. Atlas of Caesium Deposition on Europe after the Chernobyl Accident. Office for Official Publications of the European Communities, Luxembourg, pp. 1–63 ISBN 92-828-3140-X, Catalogue number CG-NA-16-733-29-C. EUR 16733.

- De Leeuw, J.W., Irene, W., Rijpstra, C., Schenck, P.A., 1981. The occurrence and identification of C_{30} , C_{31} and C_{32} alkan-1, 15-diols and alkan-15-one-1-ols in Unit I and Unit II Black Sea sediments. *Geochem. Cosmochim. Acta* 45, 2281–2285.
- Devell, L., Güntay, S., Powers, D.A., 1995. The Chernobyl Reactor Accident Source Term: Development of a Consensus View, Nuclear Energy Agency/CSNI/R(95)24. OECD Nuclear Energy Agency, Paris.
- Duplessy, J.C., Shackleton, N.J., Matthews, R.K., Prell, W., Ruddiman, W.F., Caralp, M., Hendy, C.H., 1984. ^{13}C Record of benthic foraminifera in the last interglacial ocean: implications for the carbon cycle and the global deep water circulation. *Quat. Res.* 21, 225–243.
- Gal, J.-K., Kim, J.-H., Shin, K.-H., 2018. Distribution of long chain alkyl diols along a south-north transect of the northwestern Pacific region: insights into a paleo sea surface nutrient proxy. *Org. Geochem.* 119, 80–90.
- Galbraith, E.D., Kienast, M., Jaccard, S.L., Pedersen, T.F., Brunelle, B.D., Sigman, D.M., Kiefer, T., 2008. Consistent relationship between global climate and surface nitrate utilization in the western subarctic Pacific throughout the last 500 ka. *Paleoceanography* 23, PA2212.
- Gao, L., Li, D., Ishizaka, J., Zhang, Y., Zong, H., Guo, L., 2015. Nutrient dynamics across the river-sea interface in the Changjiang (Yangtze River) estuary – East China sea region. *Limnol. Oceanogr.* 60, 2207–2221.
- Garcia, H.E., Locarnini, R.A., Boyer, T.P., Antonov, J.I., Baranova, O.K., Zweng, M.M., Reagan, J.R., Johnson, D.R., 2013. World Ocean Atlas 2013, volume 4: dissolved inorganic nutrients (phosphate, nitrate, silicate). NOAA Atlas NESDIS 76 (4), 25.
- Hendry, K.R., Rickaby, R.E.M., Hoog, J.C.M. de, Weston, K., Rehkämper, M., 2008. Cadmium and phosphate in coastal Antarctic seawater: implications for Southern Ocean nutrient cycling. *Mar. Chem.* 112, 149–157.
- Hong, G.H., Kim, S.H., Chung, C.S., Kang, D.-J., Shin, D.-H., Lee, H.J., Han, S.-J., 1997. ^{210}Pb -derived sediment accumulation rates in the southwestern East Sea (Sea of Japan). *Geo Mar. Lett.* 17, 126–132.
- Hong, G.H., Lee, S.H., Kim, S.H., Chung, C.S., Baskaran, M., 1999. Sedimentary fluxes of ^{90}Sr , ^{137}Cs , $^{239,240}Pu$ and ^{210}Pb in the East Sea (sea of Japan). *Sci. Total Environ.* 237/238, 225–240.
- Joo, H., Park, J.W., Son, S., Noh, J.H., Jeong, J.Y., Kwak, J.H., Saux-Picart, S., Choi, J.H., Kang, C.K., Lee, S.H., 2014. Long-term annual primary production in the Ulleung Basin as a biological hot spot in the East/Japan Sea. *J. Geophys. Res.: Oceans* 119, 3002–3011.
- Kim, K.J., Seung, Y.H., 1999. Formation and movement of the ESIW as modeled by MICOM. *J. Oceanogr.* 55, 369–382.
- Kim, K.R., Cho, Y.K., Kang, D.J., Ki, J.H., 2005. The origin of the Tsushima Current based on oxygen isotope measurement. *Geophys. Res. Lett.* 32, L03602.
- Kim, M., Jung, J.-H., Jin, Y.J., Han, G.M., Lee, T., Hong, S.H., Yim, U.H., Shim, W.J., Choi, D.-L., Kannan, N., 2016. Origins of suspended particulate matter based on sterol distribution in low salinity water mass observed in the offshore East China Sea. *Mar. Pollut. Bull.* 108, 281–288.
- Kroopnick, P.M., 1985. The distribution of ^{13}C of ΣCO_2 in the world oceans. *Deep Sea Research Part A. Oceanographic Research Papers* 32, 57–84.
- Kwak, J.H., Lee, S.H., Park, H.J., Choy, E.J., Jeong, H.D., Kim, K.R., Kang, C.K., 2013. Monthly measured primary and new productivities in the Ulleung Basin as a biological “hot spot” in the East/Japan Sea. *Biogeosciences* 10, 4405–4417.
- Laboratoire National Henri Becquerel (LNHB), 2017 Laboratoire National Henri Becquerel (LNHB). Decay Data Evaluation Project (DDEP). http://www.nucleide.org/DDEP_WG/DDEPdata.htm.
- Lattaud, J., Kim, J.-H., Jonge, C. De, Zell, C., Sinninghe Damsté, J.S., Schouten, S., 2017. The C_{32} alkane-1,15-diol as a tracer for riverine input in coastal seas. *Geochem. Cosmochim. Acta* 202, 146–158.
- Lea, D.W., Boyle, E.A., 1990. A 210,000-year record of barium variability in the deep northwest Atlantic Ocean. *Nature* 347, 269–272.
- Lee, K.E., Khim, B.-K., Otosaka, S., Noriki, S., 2011. Sediment trap record of alkenones from the East Sea (Japan Sea). *Org. Geochem.* 42, 255–261.
- Lee, K.E., Lee, S., Park, Y., Lee, H.J., Harada, N., 2014. Alkenone production in the East Sea/Japan Sea. *Continent. Shelf Res.* 74, 1–10.
- Lee, M.H., Lee, C.W., Moon, D.S., Kim, K.H., Boo, B.H., 1998. Distribution and inventory of fallout Pu & Cs in the sediment of the East Sea of Korea. *J. Environ. Radioact.* 41, 99–110.
- Lee, S.H., Oh, J.S., Lee, K.B., Lee, J.M., Hwang, S.H., Lee, M.K., Kwon, E.H., Kim, C.S., Choi, I.H., Yeo, I.Y., Yoon, J.Y., Im, J.M., 2018. Evaluation of abundance of artificial radionuclides in food products in South Korea and sources. *J. Environ. Radioact.* 184–185, 46–52.
- Lee, T., Hyun, J.H., Mok, J.S., Kim, D., 2008. Organic carbon accumulation and sulfate reduction rates in slope and basin sediments of the Ulleung Basin, East/Japan Sea. *Geo Mar. Lett.* 28, 153–159.
- Locarnini, R.A., Mishonov, A.V., Antonov, J.I., Boyer, T.P., Garcia, H.E., Baranova, O.K., Zweng, M.M., Paver, C.R., Reagan, J.R., Johnson, D.R., Hamilton, M., Seidov, D., 2013. World Ocean Atlas 2013. Vol. 1: temperature. In: Levitus, S., Mishonov, A., Technical (Eds.), NOAA Atlas NESDIS.
- Lynch-Stieglitz, J., Marchitto, T.M., 2014. Tracers of past ocean circulation. In: second ed. *Treatise on Geochemistry*, vol. 8. pp. 435–451.
- Marchitto, T.M., 2013. Paleoclimatology, physical and chemical proxies/Nutrient proxies. In: *Encyclopedia of Quaternary Science*, second ed. Elsevier B.V.
- Marchitto, T.M., Broecker, W.S., 2006. Deep water mass geometry in the glacial Atlantic Ocean: a review of constraints from the paleonutrient proxy Cd/Ca. *G-cubed* 7, Q12003.
- Marchitto, T.M., Oppo, D.W., Curry, W.B., 2002. Paired benthic foraminiferal Cd/Ca and Zn/Ca evidence for a greatly increased presence of Southern Ocean water in the glacial North Atlantic. *Paleoceanography* 17, 1038.
- Müller, P.J., Kirst, G., Ruhland, G., Storch, I. von, Rosell-Mele, A., 1998. Calibration of the alkenone paleotemperature index U_{37}^{K} based on core-tops from the eastern South Atlantic and the global ocean (60°N–60°S). *Geochem. Cosmochim. Acta* 62, 1757–1772.
- Nittrouer, C.A., Sternberg, R.W., Carpenter, R., Bennett, J.T., 1979. The use of Pb-210 geochronology as a sedimentological tool: application to the Washington continental shelf. *Mar. Geol.* 31, 297–316.
- Palinkas, C.M., Nittrouer, C.A., 2007. Modern sediment accumulation on the Po shelf, Adriatic Sea. *Continent. Shelf Res.* 27, 489–505.
- Park, K.-A., Chung, J.Y., Kim, K., 2004. Sea surface temperature fronts in the East (Japan) Sea and temporal variations. *Geophys. Res. Lett.* 31, L07304.
- Park, K.-A., Kim, K.-R., 2010. Unprecedented coastal upwelling in the East/Japan Sea and linkage to long-term large-scale variations. *Geophys. Res. Lett.* 37, L09603.
- Peirson, D.H., 1971. Worldwide deposition of long-lived fission products from nuclear explosions. *Nature* 234, 79–80.
- Prahl, F.G., Wakeham, S.G., 1987. Calibration of unsaturation patterns in long-chain ketone compositions for palaeotemperature assessment. *Nature* 330, 367–369.
- R Core team, 2015. R Core Team. R: A Language and Environment for Statistical Computing. R Foundation for Statistical Computing, Vienna, Austria ISBN 3-900051-07-0. <http://www.R-project.org/>.
- Rampen, S.W., Schouten, S., Koning, E., Brummer, G.J.A., Sinninghe Damsté, J.S., 2008. A 90 kyr upwelling record from the northwestern Indian Ocean using a novel long-chain diol index. *Earth Planet Sci. Lett.* 276, 207–213.
- Rampen, S.W., Schouten, S., Wakeham, S.G., Sinninghe Damsté, J.S., 2007. Seasonal and spatial variation in the sources and fluxes of long chain diols and mid-chain hydroxy methyl alkanolates in the Arabian Sea. *Org. Geochem.* 38, 165–179.
- Rampen, S.W., Willmott, V., Kim, J.H., Rodrigo-Gámiz, M., Uliana, E., Mollenhauer, G., Schefuß, E., Sinninghe Damsté, J.S., Schouten, S., 2014. Evaluation of long chain 1,14-alkyl diols in marine sediments as indicators for upwelling and temperature. *Org. Geochem.* 76, 39–47.
- Rampen, S.W., Willmott, V., Kim, J.-H., Uliana, E., Mollenhauer, G., Schefuß, E., Sinninghe Damsté, J.S., Schouten, S., 2012. Long chain 1,13- and 1,15-diols as a potential proxy for palaeotemperature reconstruction. *Geochem. Cosmochim. Acta* 84, 204–216.
- Rodrigo-Gámiz, M., Rampen, S.W., Schouten, S., Sinninghe Damsté, J.S., 2016. The impact of oxic degradation on long chain alkyl diol distributions in Arabian Sea surface sediments. *Org. Geochem.* 100, 1–9.
- Santschi, P.H., Guo, L., Asbill, S., Allison, M., Britt Kepple, A., Wen, L.S., 2001. Accumulation rates and sources of sediments and organic carbon on the Palos Verdes shelf based on radioisotopic tracers (^{137}Cs , $^{239,240}Pu$, ^{210}Pb , ^{234}Th , ^{238}U and ^{14}C). *Mar. Chem.* 73, 125–152.
- Senjyu, T., 1999. The Japan sea intermediate water; its characteristics and circulation. *J. Oceanogr.* 55, 111–122.
- Senjyu, T., Shin, H.R., Yoon, J.H., Nagano, Z., An, H.S., Byun, S.K., Lee, C.K., 2005. Deep flow field in the Japan/East Sea as deduced from direct current measurements. *Deep-Sea Res. Part II Top. Stud. Oceanogr.* 52, 1726–1741.
- Talley, L., DH, Min, V.B., Lobanov, V.A., Luchin, V.I., Ponomarev, A.N., Salyuk, A.Y., Shcherbina, P.Y., Tishchenko, I., Zhabin, 2006. Water masses and their relation to the sea's circulation. *Oceanography* 19, 32–49.
- UNSCEAR, 2000. Sources and Effects of Ionizing Radiation. United Nations Scientific Committee on the Effects of Atomic Radiation, UNSCEAR 2000 Report, New York.
- Versteegh, G.J.M., Bosch, H.-J., De Leeuw, J.W., 1997. Potential palaeoenvironmental information of C_{24} to C_{36} mid-chain diols, keto-ols and mid-chain hydroxy fatty acids: a critical review. *Org. Geochem.* 27, 1–13.
- Willmott, V., Rampen, S.W., Domack, E., Canals, M., Sinninghe Damsté, J.S., Schouten, S., 2010. Holocene changes in *Proboscia* diatom productivity in shelf waters of the northwestern Antarctic Peninsula. *Antarct. Sci.* 22, 3–10.
- Wu, Y., Zhang, J., Li, D.J., Wei, H., Lu, R.X., 2003. Isotope variability of particulate organic matter at the PN section in the East China Sea. *Biogeochemistry* 65, 31–49.
- Wu, Y., Dittmar, T., Ludwiczowski, K.U., Kattner, G., Zhang, J., Zhu, Z.Y., Koch, B.P., 2007. Tracing suspended organic nitrogen from the Yangtze River catchment into the east China sea. *Mar. Chem.* 107, 367–377.
- Yamada, K., Ishizaka, J., Nagata, H., 2005. Spatial and temporal variability of satellite primary production in the Japan Sea from 1998 to 2002. *J. Oceanogr.* 61, 857–869.
- Yoo, S., Park, J., 2009. Why is the southwest the most productive region of the East Sea/Sea of Japan? *J. Mar. Syst.* 78, 301–315.
- Zhang, X., Fan, D., Xu, J., Liu, M., Tian, Y., Chen, B., Sun, Z., Liu, W., Yang, Z., 2018. Sedimentary laminae in muddy inner continental shelf sediments of the East China Sea: formation and implications for geochronology. *Quat. Int.* 464, 343–351.